

QUANTITATIVE INTERPRETATION OF LIGHT BEAM INDUCED CURRENT CONTRAST PROFILES: BACK SIDE SURFACE INFLUENCE

G. Micard, S. Seren, G. Hahn

University of Konstanz, Department of Physics, Jacob-Burckhardt-Str. 29, 78464 Konstanz, Germany

Author for correspondence: gabriel.micard@uni-konstanz.de, Tel.: +49 7531 88 2080, Fax: +49 7531 88 3895

ABSTRACT: The quantitative interpretation of a Light Beam Induced Current (LBIC) contrast profile of a grain boundary (GB) allows the extraction of the ‘recombination strength’ of the GB, characterized by its effective surface recombination velocity (S_{eff}), and of the diffusion length (L_{diff}) of the neighboring grains. The previous fitting model developed by Donolato [1] assumed an infinite wafer thickness (h) that restricts its validity to cases where $L_{\text{diff}} \ll h$ and $1/\alpha \ll h$, with α the absorption coefficient of silicon at the considered laser wavelength. We have, however, to notice that L_{diff} could be equal or exceed h for high quality multicrystalline wafers. For these materials, the existing models present some typical type of discrepancies with the measurements that increase with increasing L_{diff} or $1/\alpha$ values. In this contribution, we will present a LBIC contrast profile model for the most simple GB configuration that takes in account the finite thickness of the wafer and consequently the back surface recombination velocity (S_b) as well as a back surface reflection coefficient (R_1). We demonstrate that for very high diffusion length materials ($L_{\text{diff}} > 500 \mu\text{m}$) the present extension can provide a local estimation of S_b that reflects the back side electrical quality. The quantitative evaluation of L_{diff} and S_{eff} is very useful for e.g. the evaluation of the effectiveness of a hydrogenation or gettering step in a solar cell process.

Keywords: Recombination, Grain boundaries, Modeling

1 INTRODUCTION

Donolato derived expressions for EBIC (electron beam induced current) and LBIC contrast profiles [1] (profile normalized to the signal infinitely far from the GB, the so-called plateau level). From this model several extensions were developed aiming at taking in account various causes of asymmetry such as: different diffusion lengths (L_{diff}) on either side of the GB [2,3], or different size of the neighboring grains which induces a different influence of the next GB on each side [4,5]. We developed recently a model that takes both aforementioned influences into account [6]. However, all these models are based on the assumption of infinite wafer thickness. This assumption restricts the validity of all these models to cases where $L_{\text{diff}} \ll h$ and $1/\alpha \ll h$, with α the absorption coefficient of silicon at the considered laser wavelength and h the thickness of the wafer.

For EBIC the spatial distribution of the generated electron hole pairs is very localized close to but significantly below the pn-junction using a beam energy of 30 keV [1]. Thus, the assumption of a localized spatial distribution ($1/\alpha \ll h$ for LBIC) is satisfied in any case for EBIC. The assumption of small L_{diff} in comparison to the thickness was satisfied with material studied in the 1980s, the time of pioneering publication in this field [1,2,4] on EBIC. There was thus no reason to develop a finite thickness model for EBIC.

However, with today’s material, the quality is much higher (higher L_{diff}) and the tendency is to reduce the wafer thickness. Thus, the assumption of infinite wafer thickness holds less and less.

While investigating LBIC, Mittiga and Cappizzi [7] pointed out the increase in accuracy in L_{diff} determination by using a more penetrative laser. We thus introduced formerly [5,6] a multiple laser wavelength fitting procedure for this purpose. However, penetration depths that are of the same order or larger than the wafer thickness can cause a severe discrepancy making the method difficult when using the present developed models.

On the other hand, it is surprising how accurate the fitting method developed with the assumptions of infinite thickness can be even in cases where the aforementioned assumption is not satisfied.

In order to investigate these aspects we performed the extension of the model of Donolato to take in account the finite thickness of the wafer, assuming a Gaussian profile for the laser beam, and derived an analytical expression for an LBIC profile that is referred here as the ‘finite thickness model’ or FTM in opposition to the ‘Infinite Thickness Model’ or ITM.

The influence of the back side is in general very weak and barely distinguishable from noise induced by the non-uniformity of the reflectance at the solar cell surface. This influence is, however, related in a complex manner to the back side parameters (back side surface recombination velocity S_b , the wafer thickness h and weakly to the back surface reflection coefficient R_b) but also to the diffusion length (L_{diff}) and to α at the considered laser wavelength.

We then provide interpretations of the discrepancies between the FTM and the ITM in terms of lateral extension of the normalized carrier density, obtained from 2-dimensional simulations while varying the aforementioned parameters. The best interpretation we found is based on the concept of effective diffusion length and on the critical back surface recombination velocity value that are used in the framework of the 1-dimensional model in the dark [8].

The comparison between FTM and ITM is also performed regarding experimental profiles on standard mc-Si solar cells, in which $L_{\text{diff}} < h$ but not necessarily $1/\alpha \ll h$, and on FZ mc-Si solar cells, in which $L_{\text{diff}} \gg h$.

We will then discuss the limitations of the present model. Finally we will discuss the possible improvements in order to increase reliability and robustness of this model.

2 THEORY AND IMPLEMENTATION OF THE ‘FINITE THICKNESS MODEL’

The theoretical contrast profile expression is obtained assuming that the collected charges in the emitter are the minority carriers driven only by diffusion. Under such conditions, the minority carrier continuity equation alone is suitable to describe the problem and thus for an n type solar cell it is expressed as.

$$\Delta p(r) - \frac{1}{L_{diff}^2} p(r) = -\frac{g(r)}{D_p} \quad (1)$$

Here D_p is the minority carrier diffusion constant, L_{diff} the minority carrier diffusion length, $g(r)$ the volume generation function and $p(r)$ the minority carrier density at point r .

The problem can be described according to the schematic shown in Fig. 1 in which we solve eq. (1).

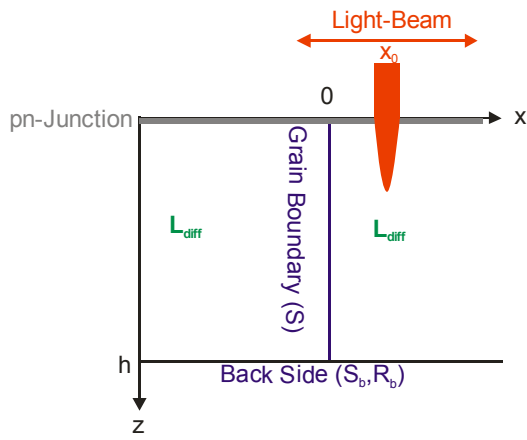


Figure 1: Schematic of the diffusion problem.

In addition to boundary conditions and assumptions described in [6], we have a boundary condition at the back side expressed as:

$$-\frac{\partial p}{\partial z} \Big|_{z=h} = s_b \cdot p \Big|_{z=h} \quad (2)$$

Introducing s_b the reduced back surface recombination velocity $s_b = S_b/D$ and h the wafer thickness.

We first look for an expression for the current collected at the junction induced by a point source located at (x_{ps}, z_{ps}) : the point source collection function Q . The fact that the problem is bounded in z leads to express Q as a generalized Fourier instead of an improper integral like in the infinite thickness model.

$$Q(x_{ps}, z_{ps}) = 2 \sum_{n=1}^{\infty} \frac{k_n}{\mu_n^2 s_b + h(k_n^2 + s_b^2)} \sin(k_n z_{ps}) \left(1 - \frac{s}{2\mu_n + s} e^{-\mu_n |z_{ps}|} \right) \quad (3)$$

With $\mu_n = (k_n^2 + L_{diff}^{-2})^{1/2}$ and s the reduced surface recombination velocity of the GB defined as $s = S/D_p$ in which k_n are the strictly positive roots of the characteristic transcendental equation:

$$\tan(k_n h) = -\frac{k_n}{s_b} \quad (4)$$

Assuming a Gaussian laser beam the projection of $g(r)$ without back reflection on the (x, z) plane is [2]

$$H(x, z) = C_1 \exp\left(-\frac{(x-x_0)^2}{\sigma^2}\right) \exp(-\alpha z) \quad (5)$$

with C_1 a constant, α the absorption coefficient at the used laser wavelength (for silicon $\alpha_{833} = 64 \text{ mm}^{-1}$, $\alpha_{910} = 27 \text{ mm}^{-1}$ and $\alpha_{980} = 9.6 \text{ mm}^{-1}$), σ the standard deviation of the beam (in our case estimated between $6 \mu\text{m}$ and $12 \mu\text{m}$ depending on the laser using a scan over a sharp edge) and x_0 the center of the beam.

Assuming a mirror-like reflection on the back surface with coefficient R_b and on the front with coefficient R_f , in a multireflection scheme H becomes

$$H(x, z) = C_2 \exp\left(-\frac{(x-x_0)^2}{\sigma^2}\right) \left[\exp(-\alpha z) + R_b \exp(-\alpha(2h-z)) \right] \quad (6)$$

with the constant

$$C_2 = C_1 \sum_{n=0}^{\infty} (R_b R_f \exp(-2\alpha h))^n = \frac{C_1}{1 - R_b R_f \exp(-2\alpha h)} \quad (7)$$

The current induced by the laser beam is calculated using this convolution product:

$$I(x_0) = q \int_{-\infty}^{\infty} \int_0^h Q(x_{ps}, z_{ps}) \cdot H(x_{ps}, x_0, z_{ps}) dz_{ps} dx_{ps} \quad (8)$$

Normalizing this current by the current obtained infinitely far from the GB, the so called plateau level I_0 , we obtain our final result:

$$\frac{I(x_0)}{I_0} = 1 - \frac{\sum_{n=1}^{\infty} A_n B_n}{\sum_{n=1}^{\infty} A_n} \quad (10)$$

with

$$A_n = \frac{k_n}{\mu_n^2 s_b + h(k_n^2 + s_b^2)} \frac{k_n}{k_n^2 + \alpha^2} \quad (11)$$

$$\times \left[1 + R_b e^{-2\alpha h} - e^{-\alpha h} \cos(hk_n) \left((1 + R_b) - \frac{\alpha}{s_b} (1 - R_b) \right) \right]$$

and

$$B_n = \frac{1}{2} \cdot \frac{s}{2\mu_n + s} \left[\frac{\exp\left(\left(\frac{\mu_n \sigma}{2}\right)^2 + \mu_n x_0\right) \operatorname{erfc}\left(\frac{\mu_n \sigma}{2} + \frac{x_0}{\sigma}\right)}{\exp\left(\left(\frac{\mu_n \sigma}{2}\right)^2 - \mu_n x_0\right) \operatorname{erfc}\left(\frac{\mu_n \sigma}{2} - \frac{x_0}{\sigma}\right)} \right] \quad (12)$$

We can observe that the front reflection coefficient R_2 is not present in this equation because the constant C_2 vanishes in the normalization process by I_0 .

An optimized algorithm was developed to compute a large number (typically 10^5) of positive roots of the characteristic equation. Because the A_n terms are independent of the beam position x_0 , they are evaluated only once at the beginning of the procedure for all computed roots and are summed up to give the denominator of the normalized current expression with

the maximum accuracy. Then, for each x_0 in the profile, a variable (and lower) number of B_n terms are evaluated considering a stopping criteria based on a maximum relative variation of the sum of $A_n B_n$ set to 10^{-7} . This procedure that was implemented in C language insures an accurate and fast computation.

The “exp(x^2)erfc(x)” term in eq. (12) requires a special evaluation procedure described in [6].

3 DISCREPANCIES BETWEEN FTM AND ITM: INFLUENCE OF PARAMETERS

3.1 One dimensional model: effective diffusion length, critical S_b and L_{diff}

In the one dimensional model in the dark one important quantity is the effective diffusion length (L_{eff}) defined as [8]:

$$L_{eff} = L_{diff} \frac{1 + S_b L_{diff} / D_p \tanh(h / L_{diff})}{S_b L_{diff} / D_p + \tanh(h / L_{diff})} \quad (13)$$

$L_{eff} = L_{diff}$ when h tends to infinity or when $S_b = D_p / L_{diff}$ independently of h . This particular value of S_b will be called S_b critical or $S_{b,crit}$.

Analogously, for a given S_b it exists a critical L_{diff} value defined as $L_{diff,crit} = D_p / S_b$.

For $S_b > S_{b,crit}$ or $L_{diff} > L_{diff,crit}$, the recombination losses at the back surface exceed the recombination loss of the volume starting from $z=h$ to infinity if the thickness would be infinite.

For $S_b < S_{b,crit}$ or $L_{diff} < L_{diff,crit}$, the recombination losses at the back surface are lower than the recombination loss of the volume starting from $z=h$ to infinity if the thickness would be infinite.

This concept, developed for a 1-dimensional model, has proven to be very useful in understanding the following discussion on the present 2-dimensional model.

The influence of S_b or L_{diff} on our profiles when comparing FTM and ITM is linked to the value of $S_{b,crit}$ and thus L_{diff} or to the value of $L_{diff,crit}$ and thus S_b , respectively.

If $L_{diff} \gg h$ and S_b not too small, eq. (13) can be simplified by taking the Taylor expansion to the first order of the hyperbolic tangent leading to.

$$L_{eff} \approx h + D_p / S_b \quad (14)$$

That means that the effective diffusion length becomes determined mainly by the thickness and in less important manner by the back sr_v but no more by L_{diff} .

3.2 influence of L_{diff} and S_b

We see in Fig. 2 that if L_{diff} is higher or lower than $L_{diff,crit}$, the FTM gives higher or lower values than the ITM, respectively.

The case of $L_{diff} = 500 \mu\text{m} < L_{diff,crit}$ is interesting because the values obtained by FTM are slightly lower close to the dip and higher in the plateau region than the values obtained by the ITM. We observe empirically that such crossing can appear when L_{diff} is close to $L_{diff,crit}$ while staying lower but never if $L_{diff} > L_{diff,crit}$.

We remark that close to the dip the discrepancy between FTM and ITM drop quickly to a low value.

For both models, the differences between profiles at $L_{diff} = 100, 200,$ and $500 \mu\text{m}$ are relatively high, and the

difference between ITM and FTM for each L_{diff} is relatively small (at least from $x_0 = 0$ to $200 \mu\text{m}$ for $L_{diff} = 500 \mu\text{m}$). On the other hand, there is only a small difference between the profiles at $L_{diff} = 500 \mu\text{m}$ and $L_{diff} = 1000 \mu\text{m}$ with the FTM while the difference keeps being large with the ITM.

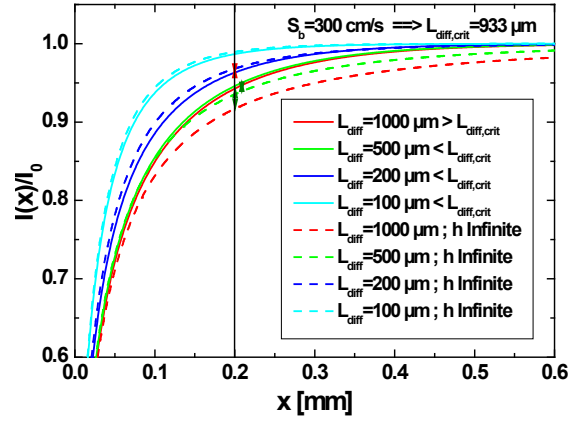


Figure 2: Simulation of GB LBIC profiles assuming $\sigma = 8 \mu\text{m}$, $S_{eff} = 10^5 \text{ cm/s}$ for a laser at $\lambda = 910 \text{ nm}$ for $L_{diff} = 100, 200, 500, 1000 \mu\text{m}$ showing the discrepancy between the FTM (with $h = 200 \mu\text{m}$, $S_b = 300 \text{ cm/s}$, and $R_b = 0.8$) and the ITM. The arrows indicate the differences between the FTM and the ITM for the 3 cases studied in Fig. 3 when the laser is located at $x_0 = 200 \mu\text{m}$. The arrow is green when the difference is positive, red when negative.

In the plateau region, the profiles obtained by the FTM converge to 1 for $x_0 > 400 \mu\text{m}$ regardless of L_{diff} . For the same region of the profile, the ITM profiles have not yet converged for $L_{diff} = 500$ and $1000 \mu\text{m}$.

In Fig. 3 we examine the carrier distribution, normalized to the maximum value, for some situations described in Fig. 2 when the laser is located at $x_0 = 200 \mu\text{m}$. This normalization allows a direct comparison of the relative extension of the normalized levels between the finite and infinite thickness case.

A broader extension of one level means that the density of carriers has the same relative value but farther from the laser position. It thus means that the same amount of carriers will recombine at the GB while the laser is farther from the GB. This will lead directly to a broadening of the profile dip. Indirectly it means that at the same position of the laser the relative level of the profile will be lower. There is thus a direct link between the carrier lateral extension when there is no GB and the width of the dip or the level at a constant laser position.

We remark first that the high density regions in Fig. 3 (red to green) have nearly identical lateral extensions in the finite or infinite thickness case. These regions will have an influence on the profile when the beam will be closer to the grain boundary than presently. The fact that they are identical gives a qualitative explanation of why the inner part of the dip is quasi identical for both models.

In order to understand the discrepancies we have then to focus on the low levels (shades of blue to pink) in which we marked a level area in light grey to ease the comparison of its lateral extension.

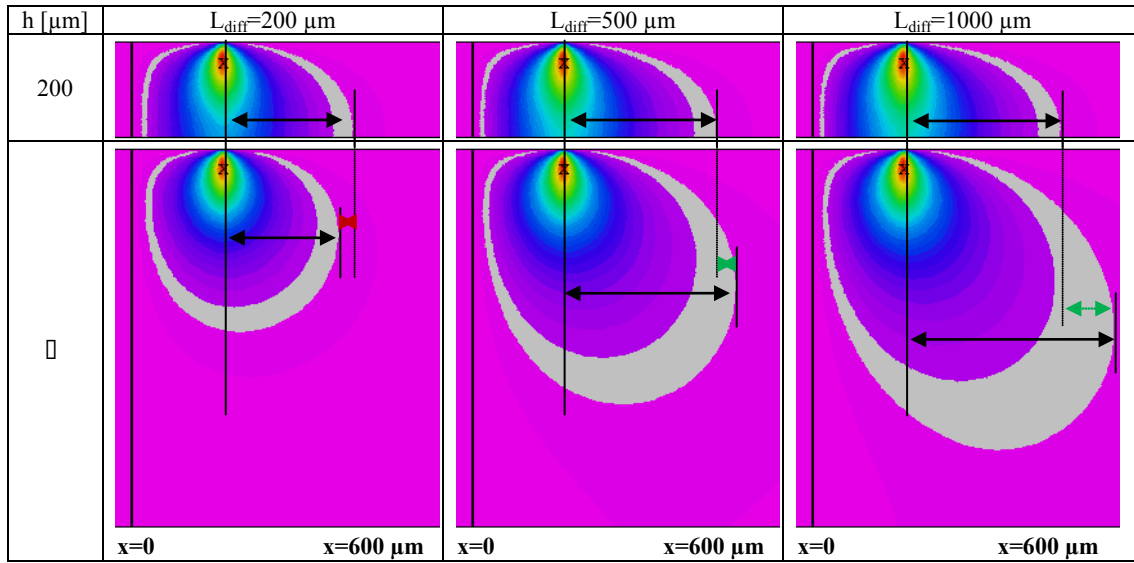


Figure 3: Comparison of the distribution of carrier density for finite ($h=200 \mu\text{m}$) and infinite thickness, and for the $L_{\text{diff}}=200$, 500, and 1000 μm when the laser beam is located at $x_0=200 \mu\text{m}$, with conditions described in Fig. 2. Particular attention is given to the maximum lateral extension of the carrier distribution at the same relative reference level (represented in light grey) for all cases. The difference between the lateral extension of the reference level between the finite and infinite thickness case is indicated by a green arrow when positive and a green one when negative.

For $L_{\text{diff}}=200 \mu\text{m}$, we observe that the lateral extension of the reference level is less pronounced for the ITM than for the FTM. This explains that the dip obtained by the FTM is broader than the one obtained by the ITM and thus that the ITM overestimate the FTM at $x_0=200 \mu\text{m}$ as we observe in Fig. 2.

In the ITM the relatively small diffusion length does not allow the carriers to diffuse far in the volume and thus the lateral extension due to the diffusion length alone is limited and comparable for both models. However, because $L_{\text{diff}} < L_{\text{diff,crit}}$ the carrier density at the back side is larger for the FTM implying that the lateral extension will be larger.

For $L_{\text{diff}}=500 \mu\text{m}$, with the ITM the carrier can extend laterally much more in depth than for the preceding case because of the longer L_{diff} . Because h becomes smaller than L_{diff} the carrier can diffuse in depth only within the wafer thickness. This apparent limitation of L_{diff} is consistent with the use of the effective diffusion length introduced in the last chapter instead of the diffusion length for the interpretation. We saw that in the case of h smaller than L_{diff} , L_{eff} depends mainly on h and on S_b but nearly not on L_{diff} . This explains that the lateral extension of carriers is comparable for $L_{\text{diff}}=500 \mu\text{m}$ and for $L_{\text{diff}}=1000 \mu\text{m} \gg h=200 \mu\text{m}$.

The phenomenon of increasing the lateral extension by increasing the carrier density because of the rather low S_b is overwhelmed by the apparent shrinkage of the diffusion length to L_{eff} that results finally in a lower lateral extension for the FTM than for the ITM. This phenomenon is further increased for $L_{\text{diff}}=1000 \mu\text{m}$.

In order to understand the influence of S_b in Fig. 4, we will investigate the lateral extension of the grey level in Fig. 5 for $h=200 \mu\text{m}$ in comparison to the infinite thickness case for various S_b .

For $S_b=10 \text{ cm/s} < S_{b,\text{crit}}$, the recombination losses at the surface are very low (lower than the recombination losses in the volume below if the carriers could extend freely). That results in an increase of the density of carriers in depth in comparison to the infinite thickness

case. This increase in depth results in a larger lateral extension and thus a broader dip as can be observed in Fig. 6.

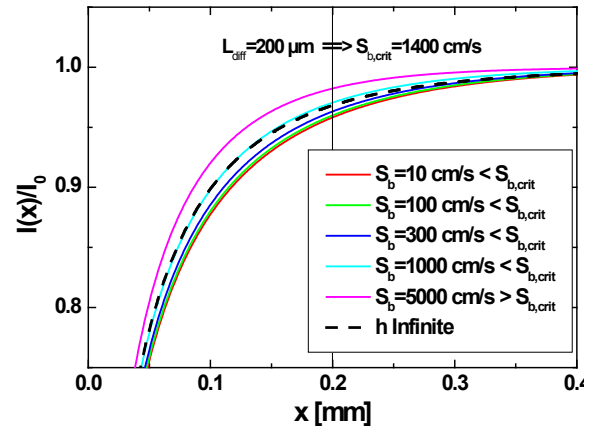


Figure 4: Simulation of GB LBIC profiles assuming $\sigma=8 \mu\text{m}$, $L_{\text{diff}}=200 \mu\text{m}$, $S_{\text{eff}}=10^5 \text{ cm/s}$ for laser at $\lambda=910 \text{ nm}$ showing the discrepancy between the FTM (with $h=200 \mu\text{m}$, $S_b=10, 100, 300, 1000, 5000 \text{ cm/s}$, and $R_b=0.8$) and the ITM.

For $S_b=300 \text{ cm/s} < S_{b,\text{crit}}$, the recombination at the back surface is higher than for the preceding case but still lower than the one of the volume below if carriers could extend freely. Thus, the lateral extension is smaller than the preceding case while still being larger than for the infinite thickness case.

For $S_b=5000 \text{ cm/s} > S_{b,\text{crit}}$, the recombination at the back surface is higher than the preceding cases but also higher than the one of the volume below if carriers could extend freely. Thus, the lateral extension is smaller than the preceding cases and the infinite thickness case as well.

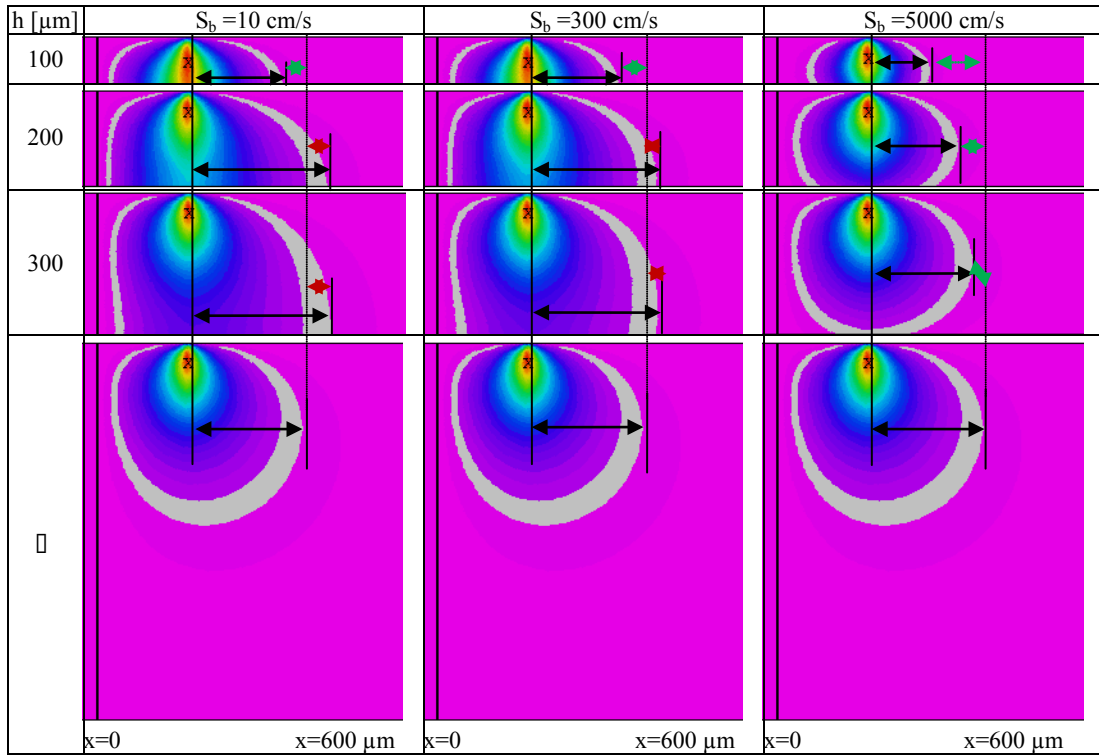


Figure 5: Comparison of the distribution of carrier density for finite ($h=200\mu\text{m}$) and infinite thickness, and for $L_{\text{diff}}=200, 500, \text{ and } 1000\mu\text{m}$ when the laser beam is located at $x_0=200\mu\text{m}$, with conditions described in Fig. 4 and Fig. 6. Particular attention is given to the maximum lateral extension of the carrier distribution at the same relative reference level (represented in light grey) for all cases. The difference between the lateral extension of the reference level between the finite and infinite thickness case is indicated by a green arrow when positive and a green one when negative.

3.3 influence of h

From the electrical point of view, the reduction of the thickness enhances the influence of the back surface and thus increases the deviations between FTM and ITM.

We can see in Fig. 6 that if $S_b=5000\text{ cm/s} > S_{b,\text{crit}}$ then the ITM underestimates the FTM on the whole profile and this phenomenon is more pronounced for decreasing thickness (see $h=100\mu\text{m}$).

When $S_b=300\text{ cm/s} < S_{b,\text{crit}}$, the ITM can under or overestimate the FTM and decreasing h tends to increase the width of regions and the value within these regions where the ITM underestimates the FTM.

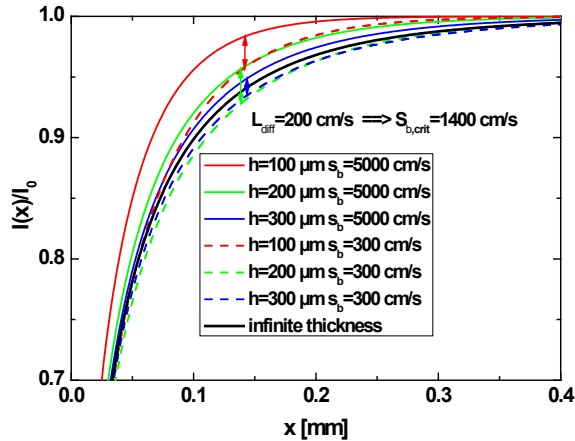


Figure 6: Simulation of GB LBIC profiles assuming $\sigma=8\mu\text{m}$, $L_{\text{diff}}=200\mu\text{m}$, $S_{\text{eff}}=10^5\text{ cm/s}$ for laser at $\lambda=910\text{ nm}$ showing the discrepancy between the FTM

(with $h=100, 200, \text{ and } 300\mu\text{m}$ for $S_b=300 \text{ and } 5000\text{ cm/s}$, and $R_b=0.8$) and the ITM.

In order to understand the influence of S_b in Fig. 6, we will observe the lateral extension of the grey level in Fig. 5 for $h=200\mu\text{m}$ in comparison to the infinite thickness case for various h and S_b .

We have shown in the last section that reducing the thickness to a value lower than L_{diff} has the effect to apparently reduce L_{diff} to L_{eff} that depends mainly on h and S_b in this case.

Starting with the case where $S_b=5000\text{ cm/s}$, we observe that a reduction of the thickness always reduces the lateral extension of the carrier density in agreement with the observations made for Fig. 6.

The fact that $S_b > S_{b,\text{crit}}$ implies that the back surface has a recombination activity that is higher than the volume below if the carriers could extend freely. However, the injection depth distribution is fixed by the wavelength of the laser and is thus independent of the wafer thickness. In the case of low thickness the recombination activity of the equivalent volume below the surface is higher because of the higher carrier density and thus reducing the thickness is further enhancing the recombination activity of the back side.

The case of least recombination losses is when the thickness is infinite when $S_b > S_{b,\text{crit}}$.

In the other case, however, the reduction of apparent diffusion length, that leads to a decrease of the lateral extension, is a concurrent phenomenon of the effect of the back surface velocity, that will lead to an increase of the lateral extension as $S_b < S_{b,\text{crit}}$.

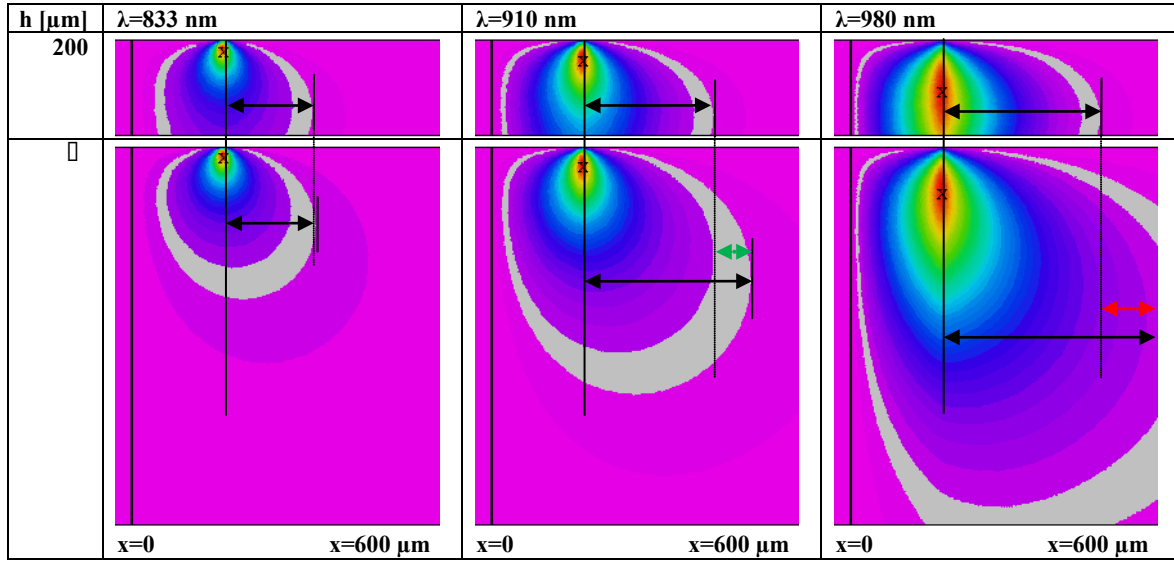


Figure 7: Comparison of the distribution of carrier density for finite ($h=200\ \mu\text{m}$) and infinite thickness, and for the three wavelengths when the laser beam is located at $x_0=200\ \mu\text{m}$, with conditions described in Fig. 8. Particular attention is given to the maximum lateral extension of the carrier distribution at the same relative reference level for all cases.

Thus, at low thickness ($h=100\ \mu\text{m}$) the apparent reduction of L_{diff} is large ($L_{\text{diff}}=200\ \mu\text{m} > L_{\text{eff}}$) and not enough compensated by the low S_b , thus the lateral extension is lower than for the infinite thickness case.

At $h=200\ \mu\text{m}$, there is not too much apparent reduction of L_{diff} ($L_{\text{diff}} \approx L_{\text{eff}}$) while the density of carriers at the back is still large. Thus, the beneficial effect of the low S_b overcomes the weak apparent reduction of L_{diff} , and the lateral extension is larger than for the infinite thickness case

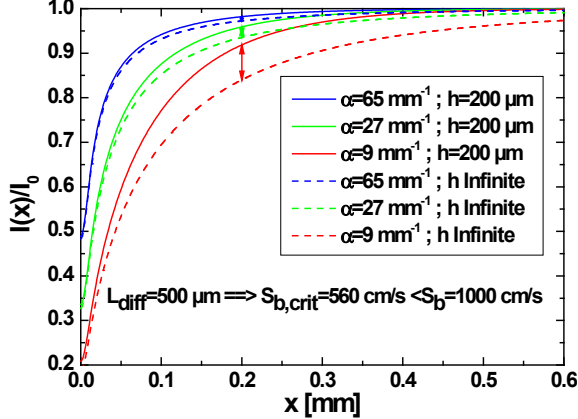


Figure 8: Simulation of GB LBIC profiles assuming $\sigma=8\ \mu\text{m}$, $S_{\text{eff}}=10^5\ \text{cm/s}$ and $L_{\text{diff}}=500\ \mu\text{m}$ for laser at $\lambda=833, 910,$ and $980\ \text{nm}$ showing the discrepancy between the finite thickness model (with $h=200\ \mu\text{m}$, $S_b=10^3\ \text{cm/s}$, and $R_b=0.8$) and the infinite thickness model. The arrows indicate the values and the differences between the finite and the infinite thickness model for the three wavelengths when the laser is located at $x_0=200\ \mu\text{m}$.

At $h=300\ \mu\text{m}$, there is no more detrimental apparent reduction of L_{diff} ($L_{\text{diff}} \approx L_{\text{eff}}$) but the density at the back surface is lower because of the higher h while all other parameters are kept constant. It thus reduces the beneficial effect of S_b . The lateral extension for

$h=200\ \mu\text{m}$ and $h=300\ \mu\text{m}$ are comparable and continuing to increase the thickness will progressively reduce the lateral extension because of no more change in L_{eff} but a reduced beneficial effect of the low S_b that decreases with the distance. Both effects will lead progressively to the infinite thickness case.

3.4 Influence of α

To investigate the absorption coefficient effect, we chose a relatively large L_{eff} of $500\ \mu\text{m}$ in order to enhance the differences between the two models, and a relatively strong S_b of $10^3\ \text{cm/s} > S_{b,\text{crit}}$. In this case the ITM always underestimates the FTM and the comparison between both models for various α is facilitated. We observe in Fig. 8 that the difference between the two models is increased while going to higher wavelengths.

One can observe from Fig. 7 that increasing the penetration depth increases the relative density in depth. Considering a large diffusion length, carriers generated in depth can travel a longer distance than the ones generated more shallowly because shallowly generated carriers are more quickly collected by the junction.

If, however, the thickness is low enough, while it changes almost nothing for carriers generated shallowly, carriers that are generated deeply can only travel laterally if they do not recombine at the back side, and thus are limited by L_{eff} in their lateral extension. This phenomenon explains in Fig. 8 that the difference between the curves obtained by the FTM is smaller than the difference between the curves obtained using the ITM.

In this framework a highly penetrative laser will induce a larger proportion of carriers generated deeply and thus the limited thickness will play a more important role. This explains the increasing difference between the two models with increasing wavelength.

We can remark that there is almost no difference in the case of the laser $\lambda=833\ \text{nm}$ corresponding to the same lateral extension of the carriers.

3.5 Influence of R_b

We observed that, except when the laser is very

penetrative ($\lambda=980$ nm) and the thickness is low ($h<200$ μm), R_b has a very weak influence on the profiles ($<0.5\%$). Indeed, a significant amount of light has to reach the back side so that its more or less high reflection modifies the generation profile. If modified significantly, the largest modification of the generated carriers is located close to the back side. Considering that carriers are collected at the front surface, a slight variation of their distribution at the back side will have an even slighter influence on the carriers collected at the front.

4 APPLICATION TO SOME REAL CASES

We first study the case of a multicrystalline Float Zone (mc-FZ) solar cell in which we extracted a linescan perpendicular to the GB from a high resolution LBIC map. In order to determine very accurately the plateau level, a large grain was investigated and a long linescan was extracted for the three different lasers of our LBIC system. A comparison is made between the FTM and the ITM in Fig. 9.

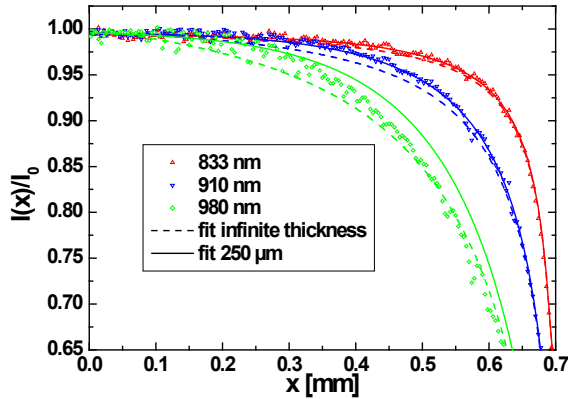


Figure 9: Comparison of fittings of an experimental normalized GB profile of a mc-FZ solar cell for the three lasers considering $\sigma_{833,910,980}=8$ μm , $L_{\text{diff}}=900$ μm , and $S_{\text{eff}}=3\cdot 10^4$ cm/s between the infinite thickness model (dashed lines) and our new finite thickness model (solid lines) with $h=250$ μm , $S_b=500$ cm/s and $R_b=0.8$ (upper zone magnified).

For the laser at $\lambda=833$ nm, the discrepancy between measurements and the two models is hardly noticeable because of the small penetration depth of the light, generating most of the carriers so close to the junction that they are directly collected and keeping the fraction that reaches the back side negligible.

For the laser at $\lambda=910$ nm, the FTM fits the upper part of the profile much more accurately than the ITM considering a $S_b=300\text{-}700$ cm/s with an average estimation around 500 cm/s .

For the laser at $\lambda=980$ nm, we observe that while the ITM fit crosses the experimental profile and is therefore unreliable, the FTM always overestimates the measured profile. This discrepancy could be attributed to a laser instability during the measurement as one can see from the large noise of the profile. Another responsible phenomenon could be the too simple mirror-like multireflection assumptions used in the model.

In Fig. 10, we study the case of a standard mc-Si material that has a smaller $L_{\text{diff}}=140$ μm $< h$. The

difference between the models is hardly noticeable for the lasers at $\lambda=833$ and 910 nm. For the laser at $\lambda=980$ nm, we observe that the fit is much better with the finite thickness model. We observe, however, that a fit considering an unrealistic value for S_b (close to 0) is hardly distinguishable from the present fit.

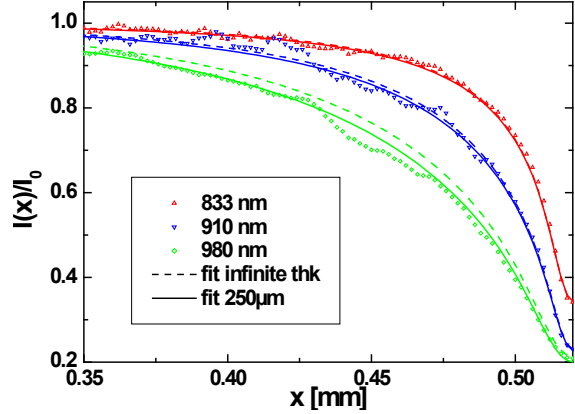


Figure 10: Comparison of fittings of an experimental normalized GB profile in standard mc-Si for the three lasers considering $\sigma_{833,910}=6$ μm and $\sigma_{980}=11$ μm , $L_{\text{diff}}=140$ μm , and $S_{\text{eff}}=6\cdot 10^3$ cm/s between the infinite thickness model (dashed lines) and our finite thickness model (solid lines) with $h=250$ μm , $S_b=100$ cm/s and $R_b=0.8$.

5 FUTURE WORK

Because the influence of S_b on the profile is weak, the fitting should be very precise and reliable to get a local approximation. This required precision is hindered by the local noise and local inhomogeneities. Because S_b influences mainly the back side density of carriers, only a laser that induces a large generation at the back (large wavelength) should be used because it induces the highest S_b influence on profile shape. This approach needs, however, a more realistic description of the back side reflection, which includes a diffuse reflection (Lambertian reflection) in addition to the direct reflection. This model cannot be integrated analytically in the present models and we thus think that a more accurate determination of S_b could be achieved by a numerical model integrating this more advanced back side reflection scheme.

We intend as well to develop an efficient optimization algorithm to fit reliably the profiles with this model.

6 CONCLUSION

An extension of the previous theories has been developed to take into account the influence of the back side. We investigated the difference between the profile shapes obtained by an infinite and a finite thickness model as a function of the most relevant parameters. The finite thickness model was applied successfully in the case of a measured LBIC contrast profile on FZ mc-Si solar cell ($L_{\text{diff}}\gg h$) and on a standard mc-Si solar cell ($L_{\text{diff}}< h$). This allows the more relevant and reliable extraction of L_{diff} when L_{diff} is high as well as an

estimation of S_b in some cases. This extension is very suitable for the investigation of GBs in high quality multicrystalline silicon particularly in the case of a reduced wafer thickness. A more realistic reflection model is, however, needed for the back side to investigate highly penetrating wavelengths and obtain more precision about S_b . The Lambertian reflection model can, however, not be straightforwardly integrated in the present model and thus a numerical approach will be implemented. This finite thickness extension will be integrated in our previously developed models [3,5,6].

7 ACKNOWLEDGEMENTS

The authors want to thank Axel Herguth and Johannes Junge for providing assistance in the high resolution LBIC maps measurements presented in this work. The authors would like to thank Robert Denk and Philippe Cance for very helpful discussions about the resolution methods of partial differential equations. Part of this work was funded by the EC in the CrystalClear (SES6-CT-2003-502583) and the German BMU in the SolarFocus (0327650H) project.

8 REFERENCES

- [1] C. Donolato, J. Appl. Phys. 54, 1314, 1983
- [2] K.L. Luke, O. von Roos, J. Appl. Phys. 55, 4275, 1984
- [3] G. Micard et al., Proc. 23rd EUPVSEC Valencia, 416, 2008
- [4] K. L. Luke, O. von Roos, J. Appl. Phys. 55, 2962, 1984
- [5] G. Micard et. al., Proc. 24th EUPVSEC Hamburg, 46, 2009
- [6] G. Micard et. al., J. Appl. Phys. 108, 034516, 2010
- [7] A. Mittiga et al., J. Appl. Phys., 62 (8), 3443, 1987
- [8] B. Fischer, PhD thesis, University of Konstanz, 2003